INTERNATIONAL JOURNAL FOR NUMERICAL METHODS IN ENGINEERING
Int. J. Numer. Meth. Engng 2017; **00**:1–27
Published online in Wiley InterScience (www.interscience.wiley.com). DOI: 10.1002/nme

Accurate and efficient a-posteriori account of geometrical imperfections in Koiter finite element analysis

G. Garcea[1*] F.S. Liguori[1] L. Leonetti[1] D. Magisano[1] A. Madeo[1]

[1] *Dipartimento di Ingegneria Informatica, Modellistica, Elettronica e Sistemistica Università della Calabria 87036 Rende (Cosenza), Italy*

SUMMARY

The Koiter method recovers the equilibrium path of an elastic structure using a reduced model, obtained by means of a quadratic asymptotic expansion of the finite element model. Its main feature is the possibility of efficiently performing sensitivity analysis by including a-posteriori the effects of the imperfections in the reduced non-linear equations. The state-of-art treatment of geometrical imperfections is accurate only for small imperfection amplitudes and linear pre-critical behavior. This work enlarges the validity of the method to a wider range of practical problems through a new approach, which accurately takes into account the imperfection without losing the benefits of the a-posteriori treatment. A mixed solid-shell finite element is used to build the discrete model. A large number of numerical tests, regarding non-linear buckling problems, modal interaction, unstable post-critical and imperfection sensitive structures, validates the proposal. Copyright © 2017 John Wiley & Sons, Ltd.

Received ...

KEY WORDS: Koiter FE method, geometrical imperfections, post-buckling, limit load, imperfection sensitivity, finite elements.

1. INTRODUCTION

Thin-walled beams and shells are commonly used as primary components in structure engineering, due to their high specific strength and stiffness, which allow weight and material economy. Their load-carrying capabilities are often determined by buckling, which often occurs for loads much lower than the failure loads of materials. The path-following strategy is the standard approach employed to analyze the non-linear elastic behavior of this kind of structure. Once the continuum problem has been discretized using the finite element (FE) method, the equilibrium path of the structure is traced step-by-step, solving a non-linear system of equations, where the unknowns are the FE degrees of freedom (DOFs) and the load factor.

*Correspondence to: Dipartimento di Ingegneria Informatica, Modellistica, Elettronica e Sistemistica. Università della Calabria, cubo 39C- 87036 Rende (Cosenza), Italy. E-mail: giovanni.garcea@unical.it
†E-mail: giovanni.garcea@unical.it

As a consequence of modal buckling interaction, shell-like structures may exhibit a very unstable post-buckling behavior and may be highly sensitive to initial imperfections [1, 2, 3, 4, 5], especially to geometrical imperfections. In light of this an *imperfection sensitivity analysis* [6, 7, 8, 9] becomes mandatory. It consists in seeking the so called *worst (detrimental)* imperfection cases, which are the shapes of the geometrical imperfections associated with the minimum limit load (safety factor). The Monte Carlo simulation generally adopted to this end may require thousands of equilibrium path evaluations [10]. The use of composite structures, which require a layup optimization [11, 12], further complicates the design process.

Standard path-following approaches, aimed at recovering the equilibrium path for a single loading case and assigned imperfections, are not suitable for this purpose because of the high computational burden of the single run [13], and are unusable if no information about the worst imperfection shapes is available. For these reasons, the FE implementation of asymptotic methods [14, 15, 16, 17, 18, 19, 20, 21, 22, 23, 24] based on Koiter's theory of elastic stability [25] has recently become [26, 27, 28, 29, 30, 31, 32, 33, 34, 35, 36] more and more attractive. The Koiter method consists of the construction of a reduced model, in which the FE model is replaced by its second order asymptotic expansion using the initial path tangent, m buckling modes and the corresponding second order modes, named quadratic correctives. In this way, once the reduced model is built, the equilibrium path of the structure can be obtained by solving the non-linear reduced system of m equations in $m+1$ unknowns, which represent the modal amplitudes and the load factor. The coefficients of the reduced system are evaluated using strain energy variations up to the $4rd$ order. Shell structures can require a very large number of FE DOFs to avoid significant discretization errors, while m is usually at most a few tens. Clearly the convenience of the method with respect to the standard path-following strategy is evident.

Since the first proposals [37, 15, 38, 6], the method has been continuously enhanced in terms of both accuracy and computational efficiency. In particular, a mixed (stress-displacement) formulation is required to avoid an *interpolation locking* phenomenon in the evaluation of the coefficients of the reduced system [6, 39, 40, 38, 41] and to make the asymptotic expansion accurate for a wider range, avoiding the *extrapolation locking* [14, 27] common in the displacement based approach and providing accurate results also for non-linear pre-critical behaviors. Geometrically exact shells and beams [42, 43] or corotational approaches [44, 32] have been proposed to achieve structural model objectivity. Both the strategies make explicit use of the rotation tensor and its highly non-linear representation. Alternatively in [26, 27], the method has been implemented exploiting the non-linear Cauchy continuum based on a Green strain measure. In this way, adopting the mixed Hellinger-Reissner variational formulation, the strain energy has a $3rd$ order only polynomial dependence on the FE DOFs with the zeroing of all the fourth order strain energy variations. The resulting asymptotic formulation appears accurate, efficient and simple.

The effects of geometrical imperfections can be included in the Koiter analysis a-priori in the FE model, like it is mandatory for the standard path-following approach. In this way the modes used in the asymptotic expansion and the coefficient of the reduced system are recomputed for each imperfection. Although this procedure is cheaper than a path-following analysis, the re-construction of the reduced model involves a linearized buckling analysis and its computational cost can still prevent a Monte Carlo simulation. On the contrary the solution of the reduced system has a very low cost (usually fractions of seconds), negligible compared to the construction of the reduced

DOI: 10.1002/nme

Due to the assumed 3rd order polynomial dependence of $\Phi[u]$ on u, it can be exactly replaced with its 3rd order Taylor expansion from a given configuration $u = u_0$, that is

$$\Phi'[u]\delta u := \left(\Phi'_0 + \Phi''_0(u-u_0) + \frac{1}{2}\Phi'''(u-u_0)^2\right)\delta u, \quad \forall \delta u \in \mathcal{T}, \tag{2}$$

where a subscript denotes, from now on, the point in which the quantities are evaluated, i.e. $\Phi'_0 \equiv \Phi'[u_0]$ and so on, while the quantity Φ''' is constant with u.

2.1.1. Fundamental path. The method starts with the evaluation of the *fundamental path* $u_f[\lambda]$ assumed as analytical in λ and approximated with its tangent in the (known) equilibrium configuration $(u_0, \lambda_0 = 0)$ as $u_f = u_0 + \lambda\hat{u}$. It is evaluated through a first order Taylor expansion in λ of Eq.(1), that is

$$\Phi''_0\hat{u}\delta u - \hat{p}\delta u = 0, \quad \forall \delta u \in \mathcal{T}. \tag{3}$$

2.1.2. Buckling loads and modes. With the adopted linear extrapolation in λ of the fundamental path, it is possible to evaluate the *bifurcation condition*, that is the singularity of the second strain energy variation, as

$$\Phi''[u_f[\lambda]]\dot{v}_i\delta u \equiv (\Phi''_0 + \lambda\Phi'''\hat{u})\dot{v}_i\delta u = 0 \; \forall \delta u \in \mathcal{T} \tag{4}$$

where $\dot{v}_i$ and λ_i are the bifurcation modes and loads. Note that the expression in Eq.(4) is exact, due to the zeroing of all the higher order energy terms, and so the buckling condition is exactly a linear eigenvalue problem [27], which provides the m bifurcation loads and modes, orthogonalized according to

$$\Phi'''\hat{u}\dot{v}_i\dot{v}_k = -\delta_{ik} \tag{5}$$

with δ_{ik} the Kronecker symbol.

2.1.3. The reduced model of the perfect structure. According to a Lyapunov-Schmidt decomposition [45], $\mathcal{U}$ is decomposed as a direct sum of the critical subspace $\mathcal{V}$ and its orthogonal complement $\mathcal{W}$, defined as

$$\mathcal{U} = \mathcal{V} \oplus \mathcal{W}, \qquad \begin{cases} \mathcal{V} = \{v : \; v = \sum_{i=1}^{m} \xi_i \dot{v}_i\} \\ \mathcal{W} = \{w : \; \Phi'''\hat{u}\dot{v}_i w = 0\} \end{cases} \tag{6}$$

where ξ_i, with $i = 1 \cdots m$ are the buckling mode amplitudes.

The space of admissible configurations, following a Galerkin approach, is limited to

$$u_d = u_f[\lambda] + v[\xi_i] + w[\lambda, \xi_i] \tag{7}$$

where the corrective term $w \in \mathcal{W}$ is assumed to be at least quadratic in λ and ξ_i and the compact notation $f[\xi_i]$ is used to denote the dependence of function f on all the ξ_i.

DOI: 10.1002/nme

Using a Ritz-Galerkin approach the equilibrium equation is imposed assuming $\dot{v}_i$ and δw as test functions, and the configuration defined by u_d, that is

$$\begin{aligned} r_w[\lambda,\xi_i] \equiv &\{\Phi'[u_d] - \lambda\hat{p}\}\delta w = 0 \\ r_k[\lambda,\xi_i] \equiv &\{\Phi'[u_d] - \lambda\hat{p}\}\dot{v}_k = 0. \end{aligned} \tag{8}$$

From the condition $r_w[\lambda,\xi_i]=0$ and using a Taylor expansion up to the 2th order in $\lambda,\xi_1,\cdots\xi_m$ we obtain the *quadratic correctives* (see [26])

$$w = \frac{1}{2}\lambda^2\hat{\hat{w}} + \frac{1}{2}\sum_{ij}\xi_i\xi_j w_{ij} \quad \begin{cases} \Phi_b''\hat{\hat{w}}\delta w = -\Phi'''\hat{u}^2\delta w \\ \Phi_b'' w_{ij}\delta w = -\Phi'''\dot{v}_i\dot{v}_j\delta w \end{cases} \quad \forall\delta w\in\mathcal{W} \tag{9}$$

where the subscript b denotes quantities evaluated in $\lambda_b\hat{u}$ and λ_b is a suitable reference value of the bifurcation load (the first bifurcation load or a mean value of the bifurcation cluster).

From the condition $r_k[\lambda,\xi_i]=0$ we obtain the reduced nonlinear system which defines the equilibrium path

$$\begin{aligned} r_k[\lambda,\xi_i] \equiv \mu_k[\lambda] + (\lambda_k-\lambda)\xi_k - \frac{1}{2}\lambda^2\sum_{i=1}^{m}\xi_i\mathcal{C}_{ik} + \frac{1}{2}\sum_{i,j=1}^{m}\xi_i\xi_j\mathcal{A}_{ijk} \\ + \frac{1}{6}\sum_{i,j,h=1}^{m}\xi_i\xi_j\xi_h\mathcal{B}_{ijhk} = 0, \quad k=1\cdots m \end{aligned} \tag{10}$$

where

$$\begin{aligned} \mathcal{A}_{ijk} =& \Phi'''\dot{v}_i\dot{v}_j\dot{v}_k \\ \mathcal{C}_{ik} =& \Phi_b''\hat{\hat{w}}w_{ik} \\ \mathcal{B}_{ijhk} =& -\Phi_b''(w_{ij}w_{hk}+w_{ih}w_{jk}+w_{ik}w_{jh}) \\ \mu_k[\lambda] =& \frac{1}{2}\lambda^2\Phi'''\hat{u}^2\dot{v}_k. \end{aligned} \tag{11}$$

Eqs.(10) are an algebraic nonlinear system of m equations in the $m+1$ variables $\lambda,\ \xi_1\cdots\xi_m$ that, due to the small size of the system, can be efficiently solved using specialized variants of the arc–length scheme. Second and third order variations of the strain energy are required for the evaluation of coefficients in Eq.(11).

2.1.4. Standard a-posteriori account of geometrical imperfections. Small imperfections, expressed by an initial displacement $\tilde{u}$, can easily be considered in the asymptotic analysis. In the current proposal [15, 40, 6, 39] the following coefficients

$$\tilde{\mu}_k := \lambda\Phi'''\hat{u}\tilde{u}\dot{v}_k \tag{12}$$

are added to Eq.(10), that is

$$r_k + \tilde{\mu}_k = 0 \tag{13}$$

and the reduced model is corrected adding $\tilde{u}$ to the expression (7)

$$u_d = \tilde{u} + u_f[\lambda] + v[\xi_i] + w[\lambda,\xi_i]. \tag{14}$$

Prepared using nmeauth.cls
DOI: 10.1002/nme

So, once the steps in Eqs.(3), (4), (9), (11) of the analysis have been performed, once and for all, small imperfections in the geometry can be taken into account by adding a few additional terms in the expression of r_k. The computational extra-cost is negligible since just the reduced nonlinear equations Eq.(10) have to be solved again for each new imperfection. In this way the method allows a low cost imperfection sensitivity analysis. In particular the reader is referred to [10] where the imperfection sensitivity analysis is performed by means of a Monte Carlo simulation showing how thousands of geometrical imperfections can be analyzed in a few minutes in order to detect the worst imperfection shape.

However, comparisons with standard path-following analyses show that the accuracy of this approach is limited to small imperfection amplitudes and structures with an almost linear pre-critical behavior. The aim of this work is, then, to improve its accuracy, making the approach suitable for a wider range of practical problems.

2.2. FEM implementation of the asymptotic approach

Denoting with a bold symbol the discrete FEM counterpart of the continuum quantities, and referring to the solid-shell finite element model presented in [26], the construction of the reduced model of the *perfect structure* consists of the following steps.

1. The fundamental path defined by Eq.(3) becomes in FE format

$$\mathbf{u}^f[\lambda] = \mathbf{u}_0 + \lambda\hat{\mathbf{u}} \;\;,\;\; \mathbf{K}_0\,\hat{\mathbf{u}} = \hat{\mathbf{p}} \;\;,\;\; \mathbf{K}_0 \equiv \mathbf{K}[\mathbf{u}_0] \tag{15a}$$

   and requires the solution of a linear system to evaluate the initial path tangent $\hat{\mathbf{u}}$.
2. The buckling modes and loads are obtained by the following eigenvalue problem

$$\mathbf{K}[\lambda]\dot{\mathbf{v}} \equiv (\mathbf{K}_0 + \lambda\mathbf{K}_1[\hat{\mathbf{u}}])\dot{\mathbf{v}} = \mathbf{0} \tag{15b}$$

   where $\mathbf{K}_0$ and $\mathbf{K}_1$ are obtained from the following energy equivalence

$$\delta\mathbf{u}^T\mathbf{K}_0\delta\mathbf{u} := \Phi_0''\delta u^2 \qquad \delta\mathbf{u}^T\mathbf{K}_1\delta\mathbf{u} = \Phi_0'''\hat{u}\delta u^2.$$

3. The $m \times (m+1)/2$ quadratic correctives FE vectors $\mathbf{w}_{ij}, \hat{\hat{\mathbf{w}}} \in \mathcal{W}$ are obtained by the solution of the linear systems ($i = 1 \dots m, j = i \dots m$)

$$\begin{aligned} \mathbf{K}_b\mathbf{w}_{ij} + \mathbf{p}_{ij} &= \mathbf{0} \\ \mathbf{K}_b\hat{\hat{\mathbf{w}}} + \mathbf{p}_{00} &= \mathbf{0} \end{aligned} \quad , \quad \forall\mathbf{w} \in \mathcal{W} \tag{15c}$$

   in which $\mathbf{K}_b \equiv \mathbf{K}[\lambda_b]$, $\mathbf{p}_{ij}, \mathbf{p}_{00}$ are defined as a function of modes $\dot{\mathbf{v}}_i$ and $\hat{\mathbf{u}}$ by the energy equivalences

$$\delta\mathbf{w}^T\mathbf{p}_{ij} = \Phi_b'''\dot{v}_j\dot{v}_j\delta w$$
$$\delta\mathbf{w}^T\mathbf{p}_{00} = \Phi_b'''\hat{u}^2\delta w.$$

DOI: 10.1002/nme

Vectors $\mathbf{w}_{ij}$ are obtained by solving the following linear systems adopting a Lagrangian multiplier approach (see [7])

$$\begin{cases} \mathbf{K}_b \mathbf{w}_{ij} + \mathbf{p}_{ij} = \mathbf{0} \\ \mathbf{w}_{ij}^T \mathbf{K}_1 \dot{\mathbf{v}}_k = 0, \qquad k = 1 \cdots m. \end{cases} \tag{15d}$$

The solution of Eq.(15d) can be obtained adopting the iterative scheme proposed in [7] which uses the already decomposed matrix $\mathbf{K}_0$. The same approach is used to evaluate $\hat{\hat{\mathbf{w}}}$.

4. Evaluation of the coefficients in Eq.(11) of reduced equilibrium system in Eq.(10) as a sum of finite element contributions.

The evaluation of the equilibrium path, to be repeated for each imperfection, requires the following steps

1. evaluation of $\tilde{\mu}_k = \lambda \Phi''' \hat{u} \tilde{u} \dot{v}_k$;
2. solution of the reduced system in Eq.(13) and drawing of the equilibrium path according to Eq.(14).

3. AN ACCURATE A-POSTERIORI ACCOUNT OF GEOMETRICAL IMPERFECTIONS

In this section the Koiter algorithm previously presented is reformulated in order to coherently consider the presence of geometrical imperfections, removing the hypothesis of linear pre-critical behavior which leads to Eq.(12). In this way it is possible to overcome the inaccuracy in the limit load evaluation observed, for example, in Fig.19 of [8]. The imperfection sensitivity analysis can still be performed in the post-processing of the Koiter method, when the geometrical imperfections are expressed as a linear combination of known shapes like, as usual, the displacement shape of the buckling modes.

3.1. The strain energy and the equilibrium path of the structure with geometrical imperfection

Using a Hellinger-Reissner variational principle the mixed strain energy $\Phi[u]$ is expressed, as usual in a FE context, as a sum of element contributions

$$\Phi[u] = \sum_e \int_{\Omega_e} \left(\mathbf{t}^T \boldsymbol{\rho}[\mathbf{d}] - \frac{1}{2} \mathbf{t}^T \mathbf{C}_\rho^{-1} \mathbf{t} \right) d\Omega_e \tag{16}$$

$\boldsymbol{\rho}[\mathbf{d}]$ and $\mathbf{t}$ are the vectors collecting the generalized strains and stresses components for the given structural model, Ω_e is the finite element domain and $\mathbf{d}$ is the displacement field and $\mathbf{C}_\rho^{-1}$ the compliance matrix of the structural model.

The strain energy of the structure for an initial imperfection characterized by an assigned displacement $\tilde{\mathbf{d}}$ and zero stress is assumed as

$$\Phi_I[u] \equiv \sum_e \int_{\Omega_e} \left(\mathbf{t}^T (\boldsymbol{\rho}[\mathbf{d}] - \boldsymbol{\rho}[\tilde{\mathbf{d}}]) - \frac{1}{2} \mathbf{t}^T \mathbf{C}_\rho^{-1} \mathbf{t} \right) d\Omega_e. \tag{17}$$

Prepared using nmeauth.cls
DOI: 10.1002/nme

Denoting with a symbol δ the variation of $\mathbf{d}$ and $\mathbf{t}$, the first variation of $\Phi_I[u]$ becomes

$$\begin{aligned}\Phi_I[u]'\delta u &= \sum_e \int_{\Omega_e} \left\{\delta\mathbf{t}^T(\boldsymbol{\rho}[\mathbf{d}] - \boldsymbol{\rho}[\tilde{\mathbf{d}}] - \mathbf{C}_\rho^{-1}\mathbf{t}) - \mathbf{t}^T\boldsymbol{\rho}'[\mathbf{d}]\delta\mathbf{d}\right\} d\Omega_e \\ &= (\Phi[u]' - \Phi'[\tilde{u}])\delta u\end{aligned} \tag{18}$$

that is the difference between the perfect and imperfect structure first order strain energy variation, being

$$\Phi'[\tilde{u}]\delta u := \sum_e \int_{\Omega_e} \delta\mathbf{t}^T\boldsymbol{\rho}[\tilde{\mathbf{d}}]d\Omega_e \tag{19}$$

the first variation of the perfect structure evaluated in $\tilde{u}$ (which has $\tilde{\mathbf{t}} = \mathbf{0}$).

The equilibrium path is obtained from the following condition

$$(\Phi[u]' - \Phi'[\tilde{u}] - \lambda p)\delta u = 0 \quad \forall\delta u \tag{20}$$

which in FE format becomes

$$\mathbf{s}[\mathbf{u}] - \tilde{\mathbf{p}} - \lambda\,\hat{\mathbf{p}} = \mathbf{0}. \tag{21}$$

In particular the internal force vector $\mathbf{s}[\mathbf{u}]$, the load vector $\hat{\mathbf{p}}$ and the imperfection vector $\tilde{\mathbf{p}}$ are defined by the energy equivalences

$$\mathbf{s}^T\delta\mathbf{u} \equiv \Phi'[u]\delta u \;\;,\;\; \hat{\mathbf{p}}^T\delta\mathbf{u} \equiv \hat{p}\,\delta u \;\;,\;\; \tilde{\mathbf{p}}^T\delta\mathbf{u} \equiv \Phi'[\tilde{u}]\delta u \;\;,\;\; \forall\,\delta\mathbf{u}. \tag{22}$$

Eq.(21) can be solved using standard path-following techniques [46, 47, 27] for an assigned imperfection $\tilde{u}$. Note that in the hybrid solid-shell FE model, the internal force vector of the imperfect structure is obtained by simply subtracting a constant vector $\tilde{\mathbf{p}}$, evaluated once and for all at the beginning of the analysis, to the internal forces vector $\mathbf{s}[\mathbf{u}]$ of the perfect structure.

3.2. The new reduced model with geometrical imperfection

The space of admissible configurations that will be used in the Lyapunov-Schmidt decomposition is obtained by adding an additional term which represents the initial imperfection, to the configuration field of the perfect structure in Eq.(7) that is

$$u_d[\lambda, \xi_i, \tilde{\xi}_i] = \tilde{u} + \lambda\hat{u} + v[\xi_i] + w[\xi_i, \tilde{\xi}_i, \lambda] \tag{23}$$

where the geometrical imperfection is assumed to be a linear combination of a known shape $\bar{u}_i$

$$\tilde{u} = \sum_{i=1}^{n} \tilde{\xi}_i\bar{u}_i. \tag{24}$$

The imperfection shapes $\bar{u}_i$ are generic and can be, for example, the displacement part of the buckling modes as well as measured geometrical imperfections. Note that, unlike the reduced model in Eq.(14), now the quadratic correctives $w[\xi_i, \tilde{\xi}_i, \lambda]$ depend on the geometrical imperfection amplitudes $\tilde{\xi}_i$.

DOI: 10.1002/nme

From now on the 3th order dependence of the strain energy on the configuration variables u (see Eq.(2)) will be exploited in order to simplify the exposition.

The residual equation (20) is firstly expanded in Taylor series starting from $\tilde{u}$, so obtaining

$$\left(\Phi''[\tilde{u}](u_d-\tilde{u})+\frac{1}{2}\Phi[\tilde{u}]'''(u_d-\tilde{u})^2-\lambda\hat{p}\right)\delta u=0.$$

The first term in previous equation is expanded again from the initial configuration of the perfect structure $(u_0=0,\lambda=0)$

$$\Phi''[\tilde{u}](u_d-\tilde{u})\delta u=(\Phi_0''+\Phi'''\tilde{u})(u_d-\tilde{u})\delta u$$

and, remembering that $\Phi_0''\hat{u}\delta u=p\delta u$

$$\left(\Phi_0''(v+w)+\frac{1}{2}\Phi'''(\lambda\hat{u}+v+w)^2+\Phi'''\tilde{u}(\lambda\hat{u}+v+w)\right)\delta u=0. \tag{25}$$

With a further Taylor expansion of $\Phi_0''(\cdot)$ starting from the $u_k=\lambda_k\hat{u}$ and letting $\Phi_k''=\Phi''[u_k]$

$$\Phi_0''(v+w)\delta u=(\Phi_k''(v+w)-\lambda_k\Phi'''\hat{u}(v+w))\delta u$$

the Eq.(25) becomes

$$\left(\Phi_k''(v+w)+(\lambda-\lambda_k)\Phi'''\hat{u}(v+w)+\frac{1}{2}\lambda^2\Phi'''\hat{u}^2+\frac{1}{2}\Phi'''(v+w)^2+\Phi'''\tilde{u}(\lambda\hat{u}+v+w)\right)\delta u=0. \tag{26}$$

It is worth mentioning again that Eq.(26) does not contain any truncation error. Furthermore note that the equilibrium condition for the structure with no imperfection is regained for $\tilde{u}=0$.

3.2.1. Projection of the equilibrium equation in the space $\mathcal{W}$. The corrective field $w\in\mathcal{W}$ is obtained by projecting Eq.(26) in direction δw, i.e. assuming $\delta u=\delta w$, and expanding it in Taylor series up to the second order in the asymptotic parameters $(\lambda,\xi_i,\tilde{\xi}_i)$. The term $\Phi_k''\dot{v}\delta w$, by exploiting the bifurcation $\Phi_i''\dot{v}_i\delta u=0$ and the orthogonality $\Phi'''\hat{u}\dot{v}_i\delta w=0$ conditions, becomes

$$\Phi_k''\dot{v}\delta w=\sum_{i=1}^{n}\xi_i\left\{\Phi_i''\dot{v}_i+(\lambda_k-\lambda_i)\Phi'''\hat{u}\dot{v}_i\right\}\delta w=0$$

that allows the simplification of the residual equation as

$$\begin{aligned}\tilde{r}_w[\xi_i,\lambda,\tilde{\xi}]\equiv\Bigg\{&\Phi''[\lambda\hat{u}]w+\frac{1}{2}\lambda^2\Phi'''\hat{u}^2\\&+\frac{1}{2}\Phi'''(v^2+2wv+w^2)+\Phi'''\tilde{u}(\lambda\hat{u}+v+w)\Bigg\}\delta w=0\end{aligned} \tag{27}$$

with $\Phi''[\lambda\hat{u}]w=\Phi_k''w+(\lambda-\lambda_k)\Phi'''\hat{u}w$.

Assuming

$$\Phi''[\lambda\hat{u}]w\approx\Phi_b''w\quad\text{with}\quad\Phi_b''\equiv\Phi''[\lambda_b\hat{u}]$$

Prepared using nmeauth.cls
DOI: 10.1002/nme

with λ_b a suitable reference value of the bifurcation cluster and maintaining only the terms of the quadratic polynomial order in $\lambda, \xi_i, \tilde{\xi}_i$ the residual equation simplifies as

$$\tilde{r}_w[\lambda, \xi_i, \tilde{\xi}_i] \equiv \left\{ \Phi_b'' w + \frac{1}{2}\lambda^2 \Phi''' \hat{u}^2 + \frac{1}{2}\Phi''' v^2 + \Phi''' \tilde{u}(\lambda \hat{u} + v) \right\} \delta w = 0. \tag{28}$$

Remembering the expression of $v[\xi_i]$, the quadratic correctives of the imperfect structure are sums of the correctives for zero imperfections of Eq.(9) and of the additional contribution due to the geometrical imperfection

$$w[\xi_i, \tilde{\xi}_i, \lambda] = \frac{1}{2}\lambda^2 \hat{\hat{w}} + \frac{1}{2}\sum_{i,j} \xi_i \xi_j \ddot{w}_{ij} + \tilde{w} \tag{29}$$

where

$$\tilde{w} = \lambda \tilde{\hat{w}} + \sum_i \xi_i \dot{\tilde{w}}_i \tag{30}$$

with

$$\tilde{\hat{w}} := \sum_j \tilde{\xi}_j \hat{\hat{w}}_j, \quad \dot{\tilde{w}}_i := \sum_j \tilde{\xi}_j \dot{\tilde{w}}_{ij}. \tag{31}$$

The terms in Eq.(31) can be evaluated, once and for all in the perfect structure step of the Koiter analysis, being known the imperfection basis, as

$$\begin{cases} \Phi_b'' \hat{\hat{w}}_i \delta w = -\Phi''' \hat{u} \bar{u}_i \delta w \\ \Phi_b'' \dot{\tilde{w}}_{ij} \delta w = -\Phi''' \dot{v}_i \bar{u}_j \delta w \end{cases} \quad \forall \delta w \in \mathcal{W}. \tag{32}$$

3.2.2. The new reduced equations with geometrical imperfection. Exploiting the orthogonality condition $\Phi''' \hat{u} w \dot{v}_k = 0$ the kth equilibrium equation, obtained assuming $\delta u = \dot{v}_k$ in Eq.(26), becomes

$$\tilde{r}_k \equiv \left((\lambda - \lambda_k)\Phi''' \hat{u} v + \frac{1}{2}\lambda^2 \Phi''' \hat{u}^2 + \frac{1}{2}\Phi'''(v+w)^2 + \Phi''' \tilde{u}(\lambda \hat{u} + v + w) \right) \dot{v}_k = 0. \tag{33}$$

Substituting the expression of w and v previously obtained, using the mode normalization condition in Eq.(5) and maintaining terms in $\lambda, \xi_i, \tilde{\xi}_i$ until the 3rd polynomial order, the equilibrium equation becomes

$$\tilde{r}_k[\lambda, \xi_i] \equiv r_k[\lambda, \xi_i] + \tilde{\mu}_k[\lambda, \xi_i] = 0, \quad k = 1 \cdots m \tag{34}$$

with $r_k[\lambda, \xi_i] = 0$ the kth reduced equilibrium equation in Eq.(10) and the new imperfection factor $\tilde{\mu}_k$ defined as

$$\begin{aligned} \tilde{\mu}_k \equiv & \sum_i \xi_i \lambda \Phi''' v_i \hat{\hat{w}} \dot{v}_k + \frac{1}{2}\sum_{ij} \xi_i \xi_j \left(\Phi''' v_i \dot{\tilde{w}}_j \dot{v}_k + \Phi''' v_j \dot{\tilde{w}}_i \dot{v}_k + \Phi''' \tilde{u} \ddot{w}_{ij} \dot{v}_k \right) \\ & + \lambda \Phi''' \tilde{u}(\hat{u} + \hat{\hat{w}}) \dot{v}_k + \sum_i \xi_i \Phi''' \tilde{u}(\dot{v}_i + \dot{\tilde{w}}_i) \dot{v}_k + \frac{1}{2}\lambda^2 \Phi''' \tilde{u} \hat{\hat{w}} \dot{v}_k. \end{aligned} \tag{35}$$

It is possible to observe that the only change, with respect to the standard reduced system in subsection 2.1.4 regards the imperfection coefficient $\tilde{\mu}_k$ which is now more complex than the one

DOI: 10.1002/nme

used in Eq.(11), which only maintains the linear contribution in λ

$$\tilde{\mu}_k = \lambda \Phi''' \hat{u} \tilde{u} \dot{v}_k$$

while the quadratic terms in λ and the terms in ξ are neglected, leading to inaccuracy as the pre-critical non-linearity increases.

Furthermore, note that the proposed reduced model assumes the following final expression

$$u_d[\lambda, \xi_i, \tilde{\xi}_i] = \tilde{u} + \lambda(\hat{u} + \tilde{\hat{w}}) + \sum_i \xi_i(\dot{v}_i + \dot{\tilde{w}}_i) + \frac{1}{2}\sum_{ij} \xi_i \xi_j \ddot{w}_{ij} + \frac{1}{2}\lambda^2 \hat{\hat{w}}. \tag{36}$$

The new correctives can be seen as a correction to the fundamental path tangent and the buckling modes of the perfect structures in order to take into account the geometrical imperfection.

3.3. FEM implementation of the proposed algorithm

The construction of the reduced model of the perfect structure presented in subsection 2.2 is completed by adding the evaluation of the new corrective after Eq.(15c)

$$\begin{cases} \mathbf{K}_b \dot{\tilde{\mathbf{w}}}_{ij} + \tilde{\mathbf{p}}_{ij} & = \mathbf{0} \\ \mathbf{K}_b \hat{\tilde{\mathbf{w}}}_i + \tilde{\mathbf{p}}_{0i} & = \mathbf{0} \end{cases}, \quad \forall \mathbf{w} \in \mathcal{W} \tag{37}$$

where

$$\delta \mathbf{w}^T \tilde{\mathbf{p}}_{ij} = \Phi_b''' \bar{v}_j \dot{u}_j \delta w \quad \delta \mathbf{w}^T \tilde{\mathbf{p}}_{0i} = \Phi_b''' \hat{u} \bar{u}_i \delta w.$$

The imperfection coefficients $\tilde{\mu}_k$ are evaluated using the expression (35) instead of (12). Once the reduced non-linear system (34) is solved, the equilibrium path is traced according to (36).

The computational cost of the Koiter method with the proposed a-posteriori account of the geometrical imperfections remains of the order of that required by a standard linearized buckling analysis, that is dominated by the factorization of the matrix $\mathbf{K}_0$. With respect to the standard approach, recalled in subsection 2.2, it is necessary to evaluate the new $m \times m$ correctives $\dot{\tilde{\mathbf{w}}}_{ij}$, and m correctives $\hat{\tilde{\mathbf{w}}}_i$ by means of the linear problem in Eq.(37) and the corresponding third order strain energy variations in Eq.(35).

4. NUMERICAL RESULTS

In this section some benchmarks are considered in order to test the accuracy of the proposed a-posteriori account of geometrical imperfection. A comparison with the different approaches is made. In particular, the numerical results report:

- the solution of the full FE model non-linear equations (21), obtained using a standard path-following technique, denoted as $Riks$ and considered the reference solution;
- the solution obtained through the Koiter method including the imperfection a-priori in the model by assuming $u_0 = \tilde{u}$ in subsection 2.1.1, which means that the reduced model is re-constructed for each imperfection while $\tilde{\mu}_k = 0$, denoted as K_0;

Prepared using nmeauth.cls
DOI: 10.1002/nme

- the solution obtained through the Koiter method using the reduced model of the perfect structure, built once and for all, and taking into account the imperfection a-posteriori in the standard way recalled in 2.1.4, denoted as K_{lin};
- the solution obtained through the Koiter method using the reduced model of the perfect structure, built once and for all, and taking into account the imperfection a-posteriori according to the new proposal described in 3.2, denoted as K_{quad}.

The geometrical imperfection is given as a linear combination of the displacement shapes of the buckling modes and its maximum displacement components, denoted as $\tilde{u}_{max}$.

DOI: 10.1002/nme

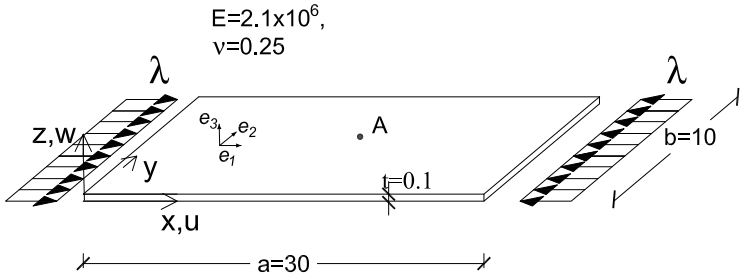

Figure 1. Simply supported plate: geometry, load and boundary conditions.

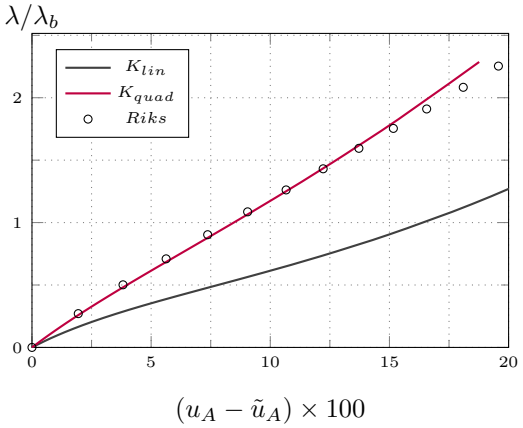

Figure 2. Simply supported plate: geometry and equilibrium paths for $\tilde{u}_{max} = t$

4.1. Simply supported plate

The first example regards a simply supported and uniformly compressed plate whose geometry, load and boundary conditions are reported in Fig.1. The imperfection shape is proportional to the first buckling mode reported in the same figure.

Fig.2 shows the equilibrium paths obtained with the different methods. In this case the proposed K_{quad} approach provides results very similar to reference $Riks$ ones, even for a large imperfection magnitude, while the standard K_{lin} approach gives a result which is completely wrong. In this case the energy terms associated with $\dot{\tilde{\mathbf{w}}}$ and $\hat{\tilde{\mathbf{w}}}$ are large also for small values of the imperfection amplitude due to the membrane hyperstaticity of the plate.

DOI: 10.1002/nme

4.2. *Cylindrical isotropic and laminated roofs*

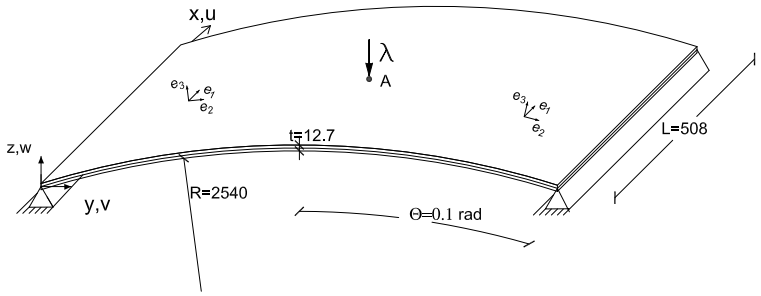

E_{11}	$E_{22}=E_{33}$	$\nu_{12}=\nu_{13}$	ν_{23}	$G_{12}=G_{13}$	G_{23}
3.3	1.1	0.25	0.25	0.66	0.44

Figure 3. Cylindrical roof subjected to a central pinching force with material properties of the ply.

The structure, whose geometry and loads are pictured in Fig.3, is a semi-cylindrical roof loaded by a central force whose curved edges are free while the straight ones are hinged. Three material configuration are studied: the first one in an isotropic material characterized by $E = 3.10275$ and Poisson ratio $\nu = 0.3$, the second and the third ones are laminated materials characterized by two different layups, $[0°/90°/0°]$ and $[90°/0°/90°]$ respectively with respect to the $\mathbf{e}_1$-axis, whose properties are reported in Fig.3. The FE mesh consists of 18×8 elements.

The imperfection shape is the displacement shape of the first buckling mode. In Figs.4, 5 and 6 the equilibrium paths and the limit loads for different values of the imperfection amplitude $\tilde{u}_{max}$ are reported. It is possible to observe how the proposed Koiter method with a-posteriori account K_{quad} furnishes accurate results for significant values of the imperfection amplitudes, very close to the a-priori account K_0 whose limit load always coincides with the $Riks$ one. Since the pre-critical behaviour is non-linear even for the structure without imperfections, the standard a-posteriori account K_{lin} fails also for very small imperfection amplitudes.

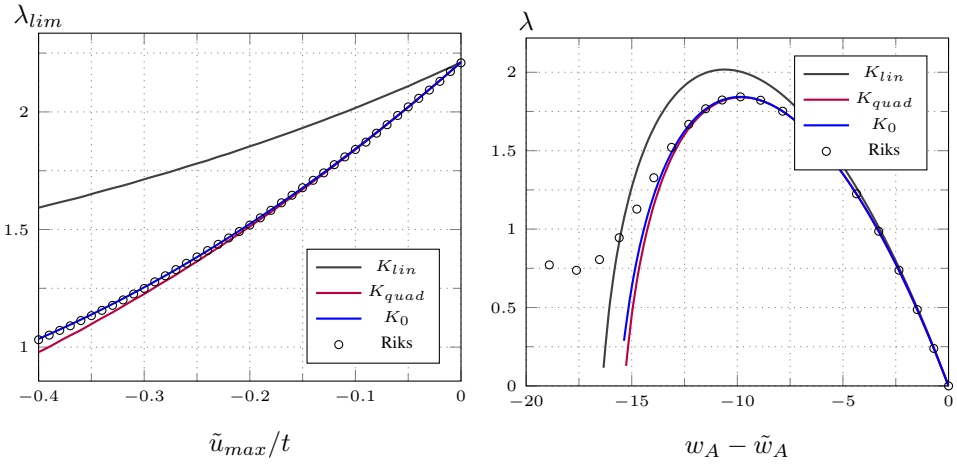

Figure 4. Cylindrical isotropic roof: limit load versus imperfection magnitude (left) and equilibrium paths for $\tilde{u}_{max} = 0.1t$ (right).

DOI: 10.1002/nme

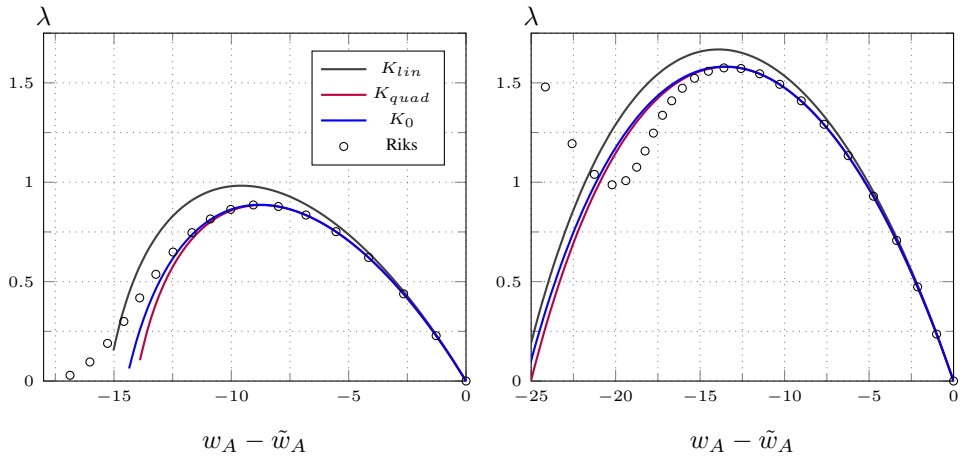

Figure 5. Cylindrical laminated roof: equilibrium paths for $u_{max} = 0.1t$ for layup [0/90/0] (left) and [90/0/90] (right).

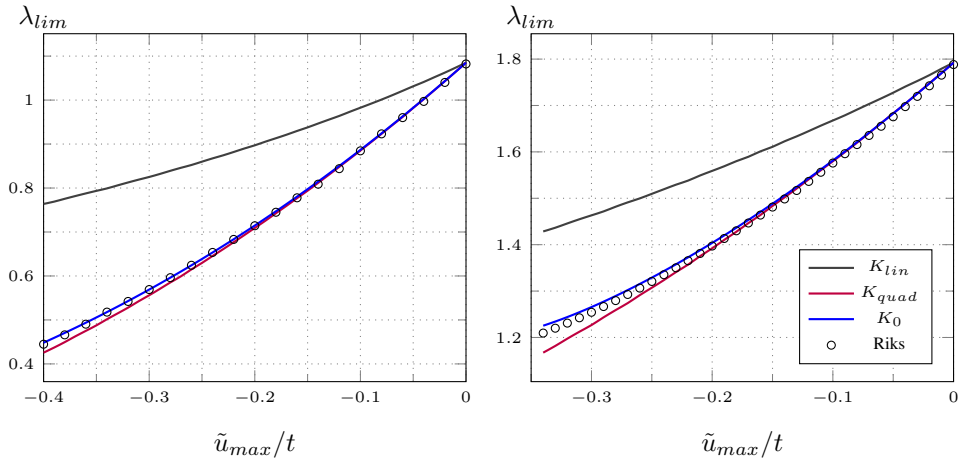

Figure 6. Cylindrical laminated roof: limit load vs imperfection magnitude for layup [0/90/0] (left) and [90/0/90] (right).

Finally it is worth noting from Fig.7 how the buckling mode corrected with $\dot{\tilde{w}}_1$, according to Eq.(36), has a shape similar to those obtained considering the imperfection a-priori in the FE model.

DOI: 10.1002/nme

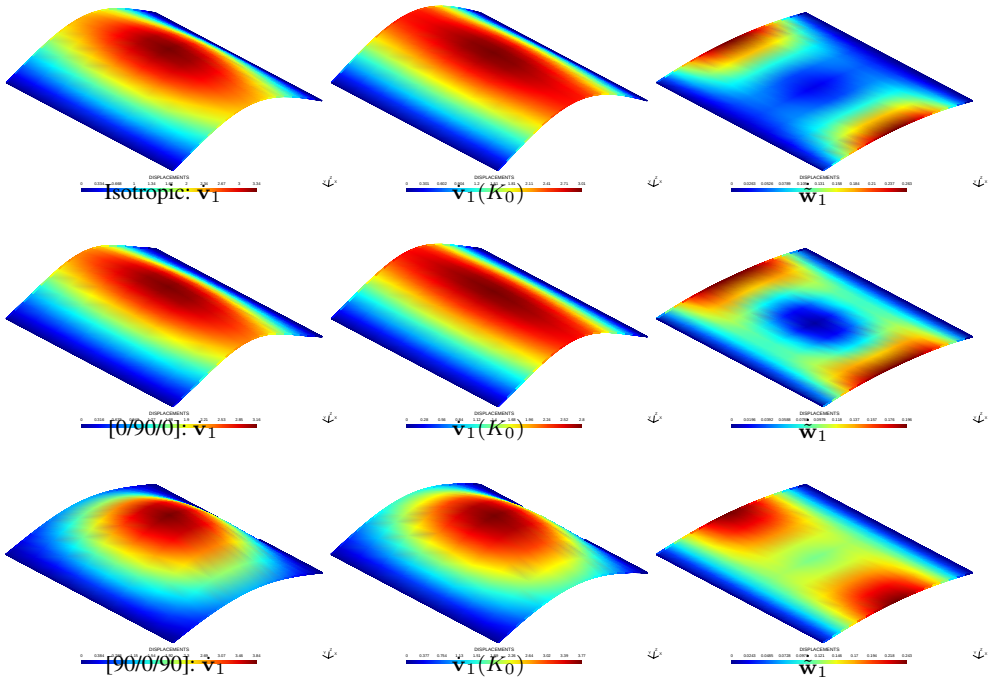

Figure 7. Cylindrical roof: bucking mode of the structure without imperfection, with $\tilde{u}_{max} = 0.2t$ and $\dot{\tilde{w}}_1$ for either isotropic, $[0/90/0]$ and $[90/0/90]$ cases.

DOI: 10.1002/nme

4.3. Compressed simply supported channel section

A simply supported channel section, whose geometry and material properties are reported in Fig.8 is now analysed with 2 different shapes of the imperfection depicted in Fig.13: the first one is the displacement shape of the first buckling mode (flexural), the second one corresponds to the displacement shape of the 3rd buckling mode (local with 13 half-waves). The structure exhibits buckling mode interaction phenomena.

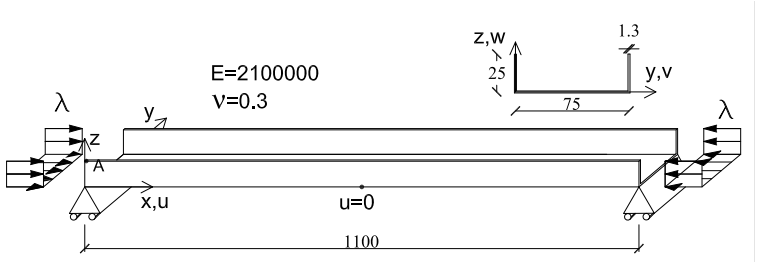

Figure 8. Compressed simply supported channel section with material properties.

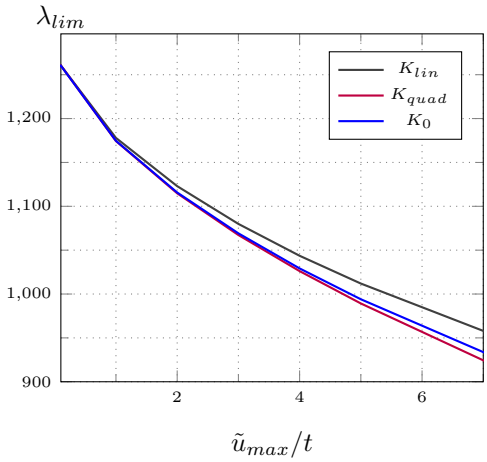

Figure 9. C-section: limit load versus imperfection magnitude for flexural imperfection.

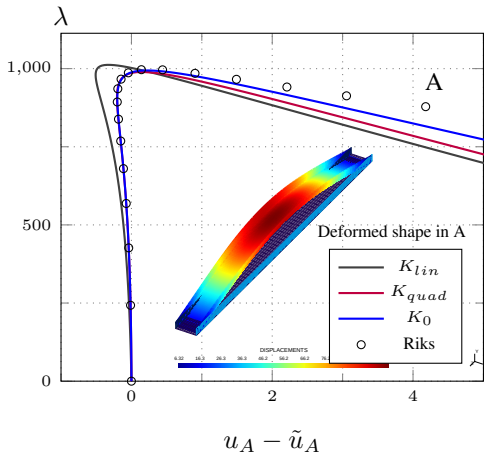

Figure 10. C-section: equilibrium paths for first buckling shape imperfection and $u_{max} = 5t$ (upwards).

In Fig.9 it is reported how the limit loads change with the amplitude of the first imperfection, while Fig.10 shows the equilibrium paths for $\tilde{u}_{max} = 5t$. In Fig.11 the buckling modes and correctives for K_0 and K_{quad} are reported. It can be observed how the buckling mode of the imperfect structure presents a shortening, while for the perfect structure presents a similar shape by summing its first buckling mode $\dot{v}_1$ and the corrective $\dot{\tilde{w}}_1$, according to Eq.(36). The good behaviour in the evaluation of the limit point of K_{quad} is evident while K_{lin} presents significant errors in the equilibrium path evaluation notwithstanding the fairly accurate value of the limit load.

In Fig.12 the equilibrium paths and the deformed shapes in two equilibrium points for the second imperfection, are presented. The corresponding mode shapes and how they change with the imperfection are reported in Fig.13. Also in this case the good behaviour of the proposal K_{quad}, compared to K_{lin}, is evident.

DOI: 10.1002/nme

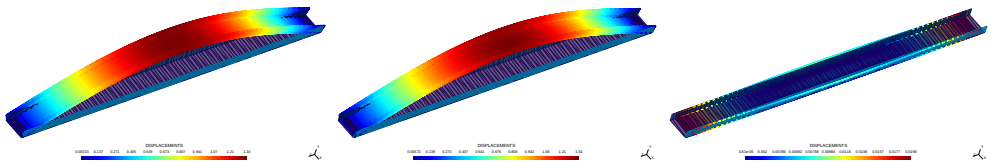

Figure 11. C-section: buckling mode of the structure without imperfection (left), with an imperfection in the direction of the first buckling mode of amplitude $\tilde{u}_{max} = 5t$ (centre) and the relative $\tilde{\dot{w}}_1$ (right, displacement factor 10).

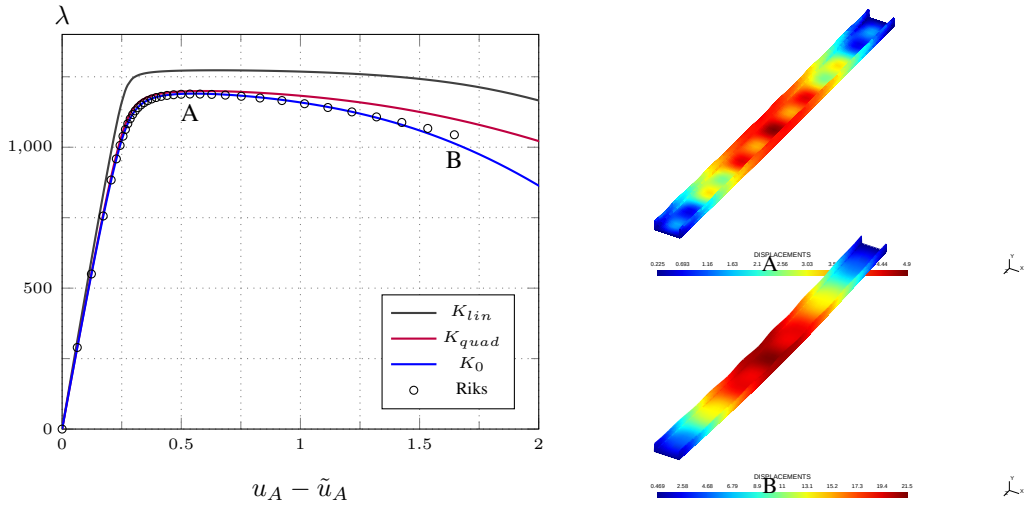

Figure 12. C-section: equilibrium paths for third buckling shape imperfection and $\tilde{u}_{max} = -0.5t$. 12 modes have been considered in asymptotic analysis.

DOI: 10.1002/nme

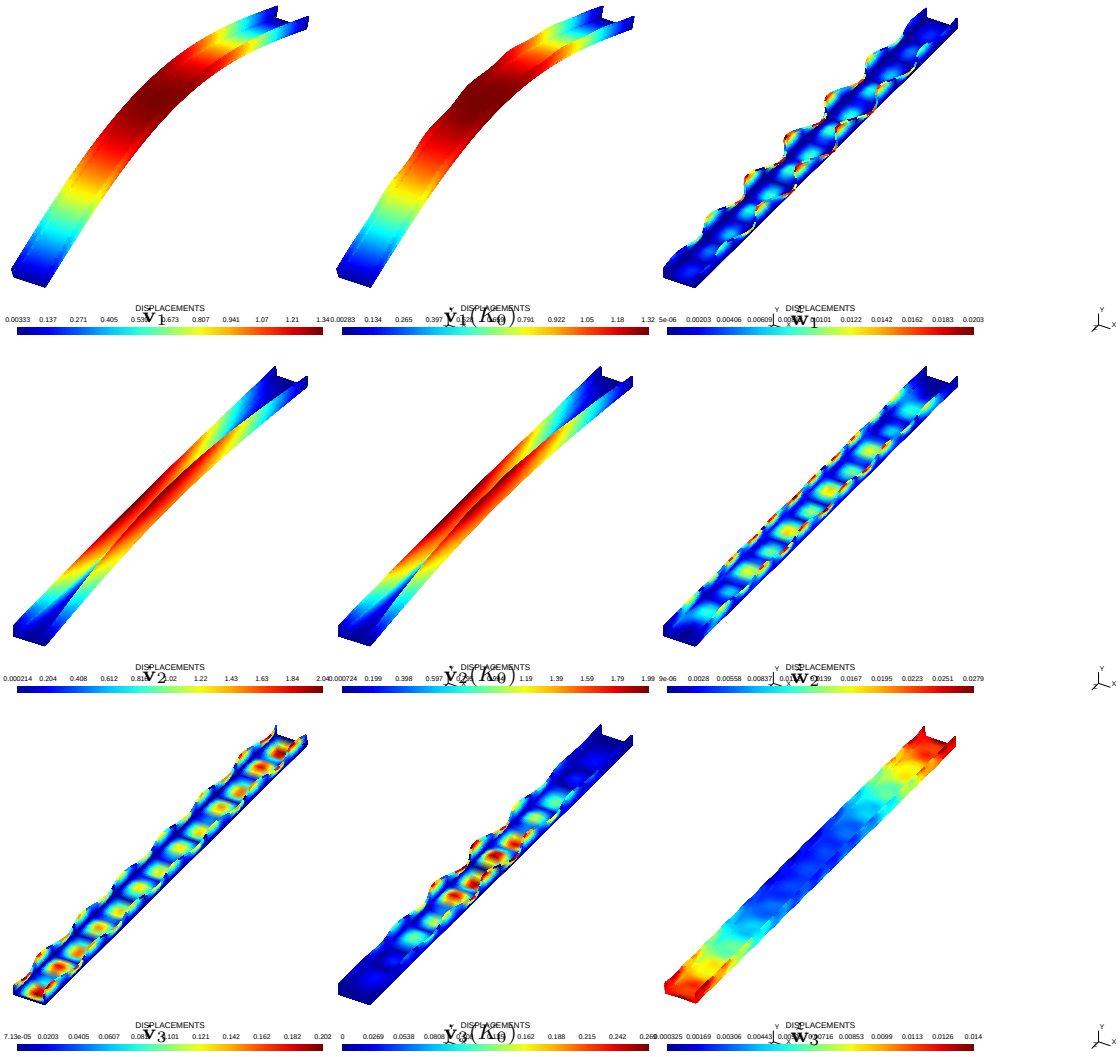

Figure 13. C-section: first, second and third buckling modes of the structure without imperfection, with $\tilde{u}_{max} = 0.5t$ in the direction of the third buckling mode and $\tilde{\hat{w}}$ (displacement factor 10).

DOI: 10.1002/nme

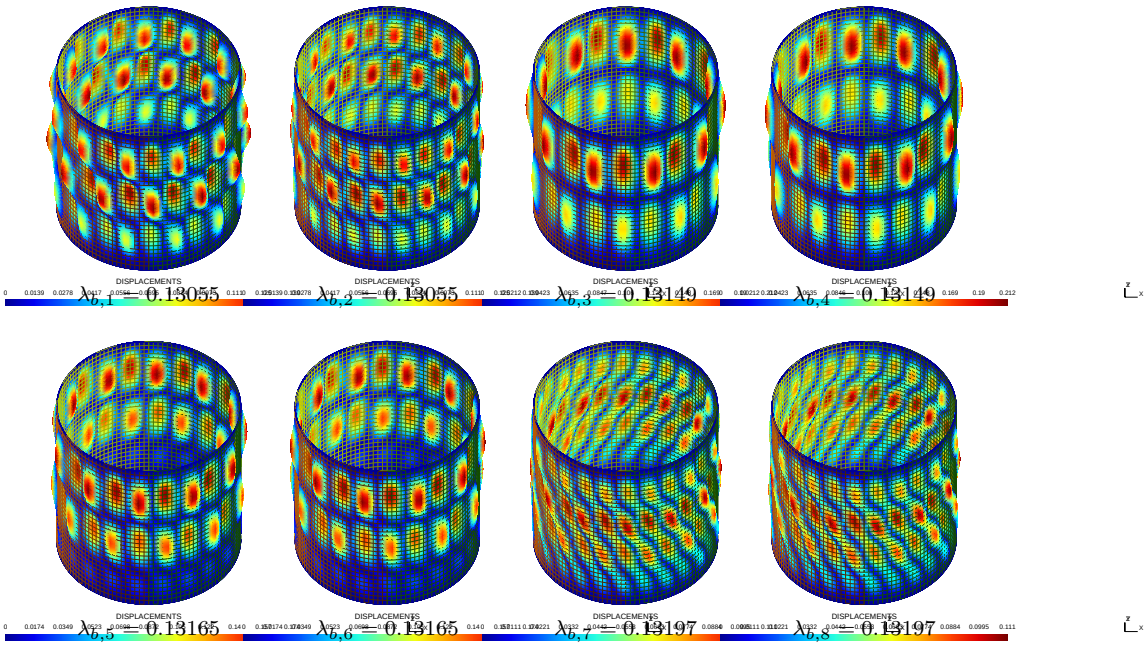

Figure 14. Cylinder Z33: first 8 buckling modes of the structure without imperfection.

4.4. Cylinder

The test regards a compressed composite cylinder. The stacking sequence is $_{in}[0/0/19/-19/37/-37/45/-45/51/-51]_{out}$ with the rotation measured from the cylinder axis with respect to the outward normal. The height is $510\,mm$, the radius is $R = 250\,mm$, the thickness $t = 1.25\,mm$. The ply properties are $E_1 = 123.6$, $E_2 = E_3 = 8.7$, $\nu_{12} = 0.32$, $\nu_{13} = \nu_{23} = 0$, $G_{12} = G_{13} = G_{23} = 5.7$. The cylinder is labelled Z33 in the literature [10, 48] and has been used as a benchmark case of imperfection sensitivity. The cylinder is clamped on the top and bottom, excluding the axial displacement at the top edge where an uniform distributed load is applied. The displacement in the load direction of a node located at the top of the structure, and labelled w_A, has been chosen as control parameter in the equilibrium path representation. Some of the buckling modes of the perfect structure are plotted in Fig.14 while those of the imperfect one and the corresponding correctives $\dot{\hat{w}}_k$ for a geometrical imperfection in the direction of $\dot{v}_1$ are reported, respectively in Fig.16 and Fig.17. The equilibrium path and the deformed shape at the limit point, for $\tilde{u}_{max} = 0.2t$ are plotted in Fig.15 while the limit load values for all the methods are presented in Tab.I. Finally in Fig.18 there are the equilibrium paths for a different imperfection shape and $\tilde{u}_{max} = 0.2t$. Also in this case the limit loads evaluated with the different formulations are reported in Tab.I. The K_{quad} approach always exhibits greater accuracy than K_{lin} for both the imperfection shapes.

imp. direction	K_{lin}	K_{quad}	K_0	$Riks$
$\dot{\mathbf{v}}_1$	0.0831	0.0732	0.0759	0.0769
$\dot{\mathbf{v}}_1 + \dot{\mathbf{v}}_2 + \dot{\mathbf{v}}_3$	0.0929	0.0868	0.0825	0.0826

Table I. Cylinder: limit load to imperfection direction for several methods and imperfection amplitudes $\tilde{u}_{max} = 0.2t$.

DOI: 10.1002/nme

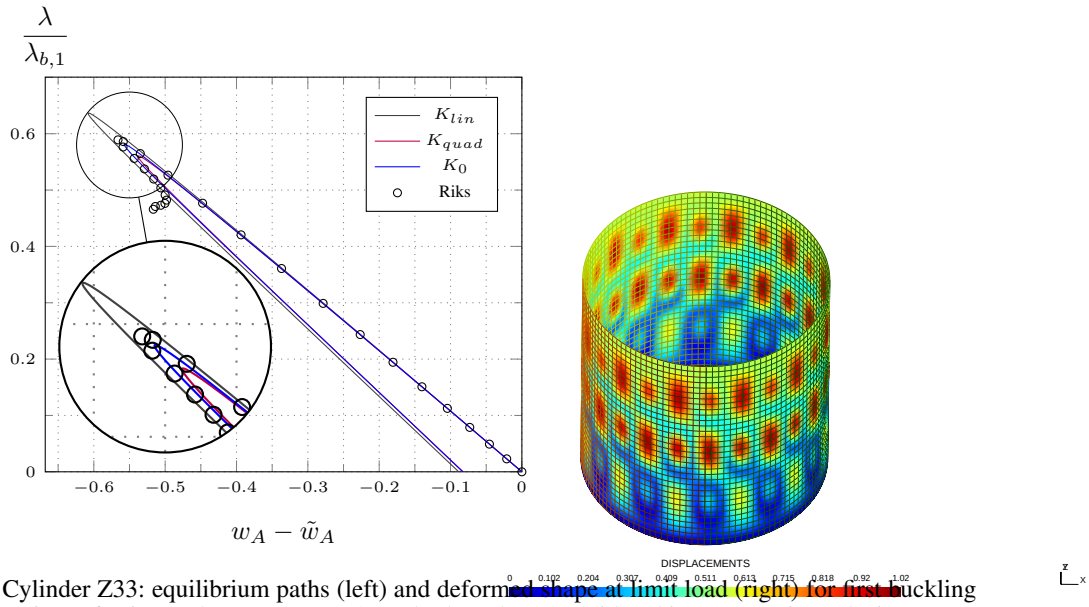

Figure 15. Cylinder Z33: equilibrium paths (left) and deformed shape at limit load (right) for first buckling shape imperfection and $\tilde{u}_{max} = 0.2t$. 8 modes have been considered in asymptotic analysis.

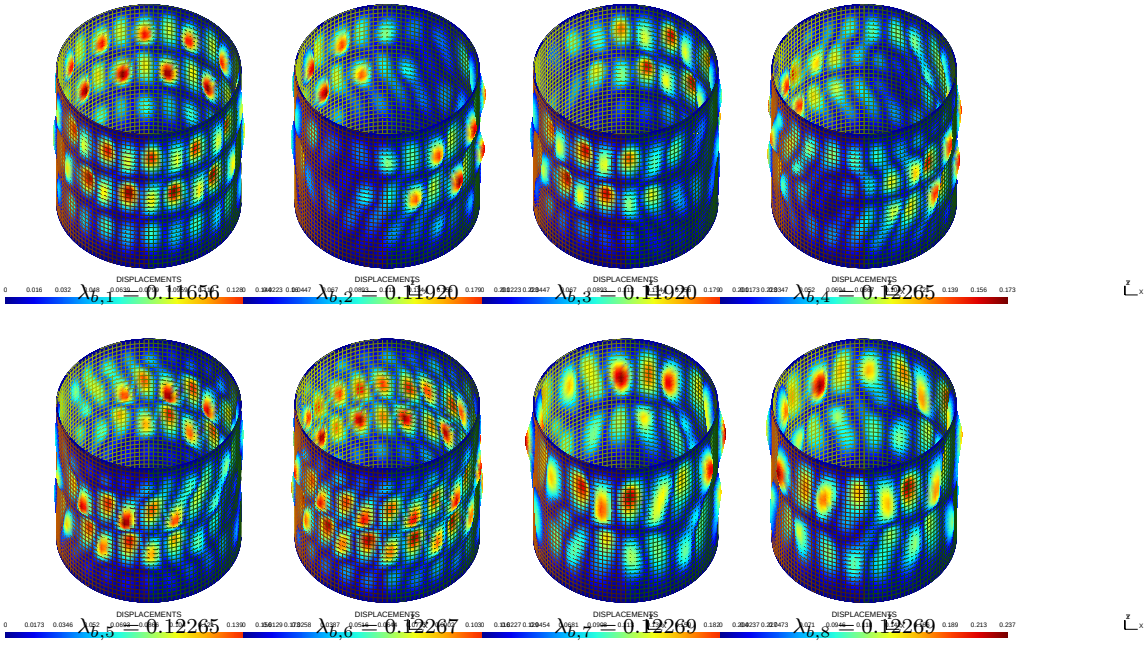

Figure 16. Cylinder Z33: $\dot{\mathbf{u}}$ in the case of imperfection along the first buckling mode and maximum amplitude $\tilde{u}_{max} = 0.2t$.

Prepared using nmeauth.cls
DOI: 10.1002/nme

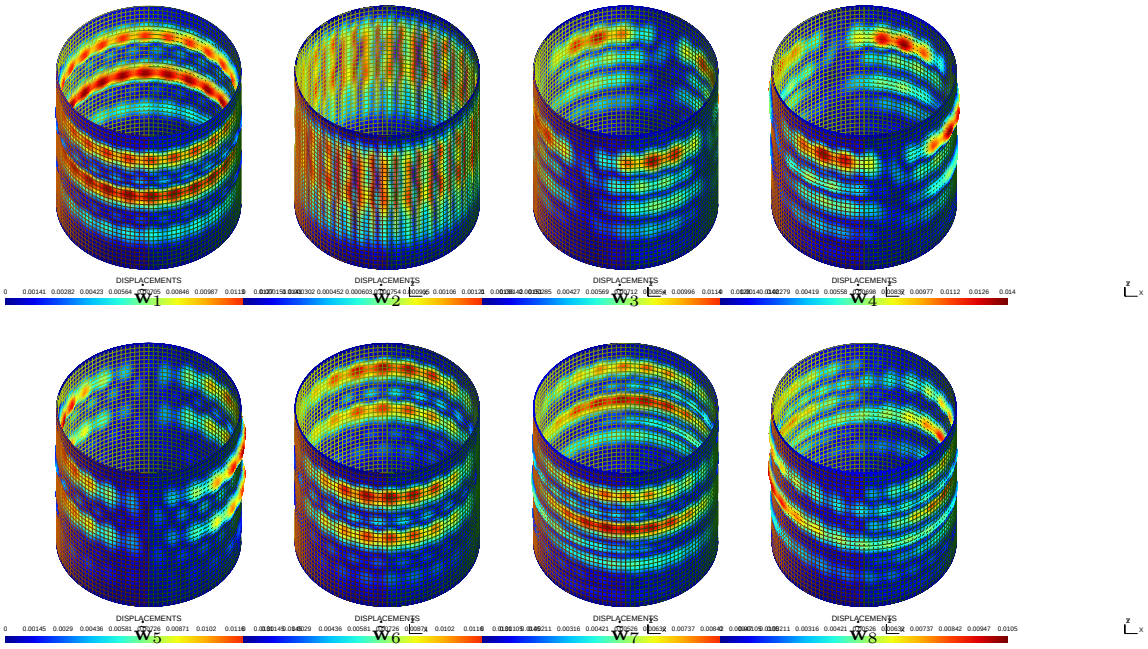

Figure 17. Cylinder Z33: $\dot{\tilde{\mathbf{w}}}$ in the case of imperfection along the first buckling mode and maximum amplitude $\tilde{u}_{max} = 0.2t$. The displacement scale is ten times bigger than the one used in the buckling mode representation.

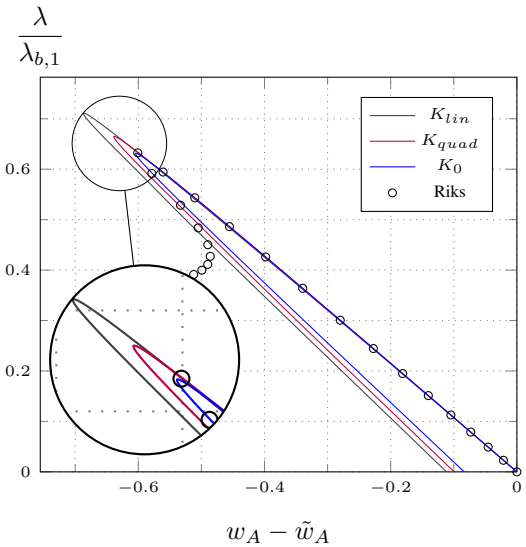

Figure 18. Cylinder Z33: equilibrium paths for imperfection: $\tilde{\mathbf{u}} = \dot{\mathbf{v}}_1 + \dot{\mathbf{v}}_2 + \dot{\mathbf{v}}_3$ and $\tilde{u}_{max} = 0.2t$. 8 modes have been considered in asymptotic analysis.

DOI: 10.1002/nme

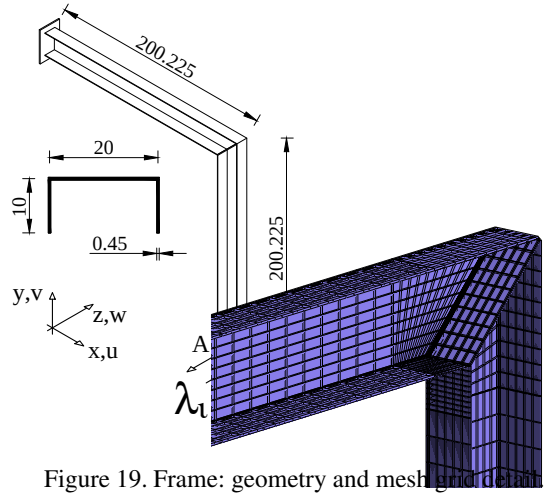

Figure 19. Frame: geometry and mesh grid details.

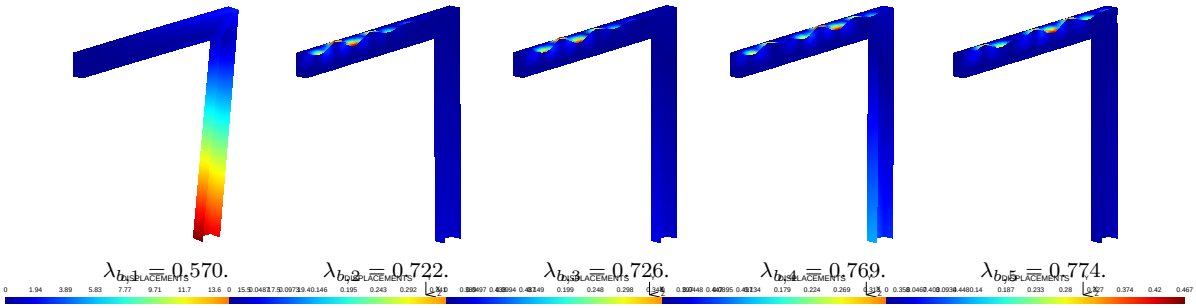

Figure 20. Frame: First 5 buckling modes of the structure without geometrical imperfections.

4.5. Frame

The last test regards the frame reported in Fig.19.

The first 5 buckling modes of the perfect structure are reported in Fig.20, while the limit load versus imperfection amplitude curve for a geometrical imperfection with the shape of the second buckling mode and the equilibrium path for $\tilde{u}_{max} = 0.4t$ are reported in Fig.21. In the same figure, the equilibrium path of the structure without imperfections is presented, in order to point out the strong imperfection sensitivity of the frame and the modal interaction phenomenon. Even in this last case the proposal K_{quad} provides very accurate results with a limit point which coincides with the a-priori account K_0 and $Riks$ solution, while inaccuracies occur for K_{lin}.

DOI: 10.1002/nme

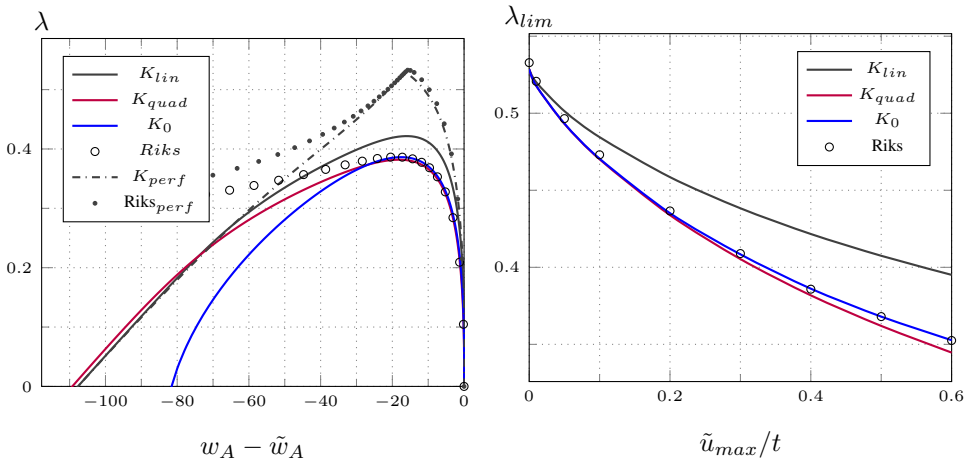

Figure 21. Frame: equilibrium paths for geometrical imperfection along the second buckling mode and $\tilde{u}_{max} = 0.4t$ (left) and magnitude imperfection sensitivity (right).

DOI: 10.1002/nme

5. CONCLUSION

A new strategy to include, a-posteriori, geometrical imperfections in Koiter analysis is proposed in this paper. The main idea is to correct the linear modes of the perfect structure reduced model using additional corrective modes, which take into account the imperfections. The reduced system of the imperfect structure is obtained starting from the system of the perfect structure by adding some terms, which coherently consider the geometrical imperfection up to the second order. In this way, the Koiter method with a-posteriori account of the imperfections becomes accurate even for pre-critical non-linearities and significant imperfection amplitudes, making the approach suitable for a wide range of practical problems.

A large number of numerical tests, regarding shell structures in both isotropic or laminated materials and also presenting complex behavior characterized by almost coincident buckling loads and pre-critical non-linearities, validates the proposal. The limit load provided by the new a-posteriori account is very close to the path-following reference solution and to that provided by the Koiter method with the imperfection included a-priori in the model.

Finally, this work confirms that the Koiter method is definitely a suitable tool for analyzing imperfection sensitive structures and shows that the a-posteriori account of the geometrical imperfections is not only a possibility, but also an accurate and efficient choice.

References

1. Dinis P, Camotim D. Post-buckling behaviour and strength of cold-formed steel lipped channel columns experiencing distortional/global interaction. *Computers and Structures* 2011; **89**(3-4):422–434, doi: 10.1016/j.compstruc.2010.11.015.
2. Dinis PB, Camotim D. Cold-formed steel columns undergoing local-distortional coupling: Behaviour and direct strength prediction against interactive failure. *Computer & Structures* JAN 15 2015; **147**(SI):181–208, doi: 10.1016/j.compstruc.2014.09.012.
3. Khakimova R, Warren CJ, Zimmermann R, Castro SGP, Arbelo MA, Degenhardt R. The single perturbation load approach applied to imperfection sensitive conical composite structures. *Thin-Walled Structures* NOV 2014; **84**:369–377, doi:10.1016/j.tws.2014.07.005.
4. Castro SGP, Zimmermann R, Arbelo MA, Khakimova R, Hilburger MW, Degenhardt R. Geometric imperfections and lower-bound methods used to calculate knock-down factors for axially compressed composite cylindrical shells. *Thin-Walled Structures* JAN 2014; **74**:118–132, doi:10.1016/j.tws.2013.08.011.
5. Arbelo MA, Degenhardt R, Castro SGP, Zimmermann R. Numerical characterization of imperfection sensitive composite structures. *Composite Structures* FEB 2014; **108**:295–303, doi:10.1016/j.compstruct.2013.09.041.
6. Casciaro R. Computational Asymptotic Post-Buckling Analysis of Slender Elastic Structures. *CISM Courses and Lectures NO. 470* 2005; :.
7. Casciaro R, Garcea G, Attanasio G, Giordano F. Perturbation approach to elastic post-buckling analysis. *Computers & Structures* 1998; **66**(5):585–595.
8. Barbero E, Madeo A, Zagari G, Zinno R, Zucco G. Imperfection sensitivity analysis of laminated folded plates. *Thin-Walled Structures* 2015; **90**:128 – 139, doi:http://dx.doi.org/10.1016/j.tws.2015.01.017.
9. Dubina D, Ungureanu V. Instability mode interaction: From Van der Neut model to ECBL approach. *Thin-Walled Structures* 2014; **81**:39–49, doi:10.1016/j.tws.2013.10.014.
10. Zagari G, Zucco G, Madeo A, Ungureanu V, Zinno R, Dubina D. Evaluation of the erosion of critical buckling load of cold-formed steel members in compression based on Koiter asymptotic analysis. *Thin-Walled Structures* 2016; **108**:193–204, doi:10.1016/j.tws.2016.08.011.
11. Lindgaard E, Lund E, Rasmussen K. Nonlinear buckling optimization of composite structures considering "worst" shape imperfections. *International Journal of Solids and Structures* 2010; **47**(22–23):3186 – 3202, doi: http://dx.doi.org/10.1016/j.ijsolstr.2010.07.020.

DOI: 10.1002/nme

12. Henrichsen S, Weaver P, Lindgaard E, Lund E. Post-buckling optimization of composite structures using Koiter's method. *International Journal for Numerical Methods in Engineering* 2016; doi:10.1002/nme.5239.
13. Papadopoulos V, Soimiris G, Papadrakakis M. Buckling analysis of I-section portal frames with stochastic imperfections. *Engineering Structures* FEB 2013; **47**(SI):54–66, doi:10.1016/j.engstruct.2012.09.009.
14. Garcea G, Salerno G, Casciaro R. Extrapolation locking and its sanitization in Koiter's asymptotic analysis. *Computer Methods in Applied Mechanics and Engineering* 1999; **180**(1-2):137–167.
15. Lanzo AD, Garcea G, Casciaro R. Asymptotic post-buckling analysis of rectangular plates by HC finite elements. *International Journal for Numerical Methods in Engineering* 1995; **38**(14):2325–2345.
16. Rahman T, Jansen E. Finite element based coupled mode initial post-buckling analysis of a composite cylindrical shell. *Thin-Walled Structures* 2010; **48**(1):25–32, doi:10.1016/j.tws.2009.08.003.
17. Barbero E, Godoy L, Raftoyiannis I. Finite elements for three-mode interaction in buckling analysis. *International Journal for Numerical Methods in Engineering* 1996; **39**(3):469–488. Cited By 14.
18. Flores F, Godoy L. Elastic post-buckling analysis via finite element and perturbation techniques. Part 1: Formulation. *International Journal for Numerical Methods in Engineering* 1992; **33**(9):1775–1794.
19. Barbero E, Raftoyiannis I, Godoy L. Finite elements for post-buckling analysis. II-Application to composite plate assemblies. *Computers and Structures* 1995; **56**(6):1019–1028.
20. Boutyour E, Zahrouni H, Potier-Ferry M, Boudi M. Asymptotic-numerical method for buckling analysis of shell structures with large rotations. *Journal of Computational and Applied Mathematics* 2004; **168**(1-2):77–85, doi: 10.1016/j.cam.2003.05.010.
21. Silvestre N, Camotim D. Asymptotic-numerical method to analyze the postbuckling behavior, imperfection-sensitivity, and mode interaction in frames. *Journal of Engineering Mechanics* 2005; **131**(6):617–632, doi: 10.1061/(ASCE)0733-9399(2005)131:6(617).
22. Schafer B, Graham-Brady L. Stochastic post-buckling of frames using Koiter's method. *International Journal of Structural Stability and Dynamics* 2006; **6**(3):333–358, doi:10.1142/S0219455406001976.
23. Chen H, Virgin L. Finite element analysis of post-buckling dynamics in plates-Part I: An asymptotic approach. *International Journal of Solids and Structures* 2006; **43**(13):3983–4007, doi:10.1016/j.ijsolstr.2005.04.036.
24. Rizzi NL, Varano V, Gabriele S. Initial postbuckling behavior of thin-walled frames under mode interaction. *Thin-Walled Structures* 2013; **68**:124 – 134, doi:http://dx.doi.org/10.1016/j.tws.2013.03.004.
25. Koiter W. *On the stability of elastic equilibrium*. English transl. nasa tt-f10, 883 (1967) and affdl-tr70-25 (1970) edn., Techische Hooge School at Delft, 1945.
26. Magisano D, Leonetti L, Garcea G. Koiter asymptotic analysis of multilayered composite structures using mixed solid-shell finite elements. *Composite Structures* 2016; **154**:296–308, doi:10.1016/j.compstruct.2016.07.046.
27. Magisano D, Leonetti L, Garcea G. Advantages of the mixed format in geometrically nonlinear analysis of beams and shells using solid finite elements. *International Journal for Numerical Methods in Engineering* 2017; **109**(9):1237–1262, doi:10.1002/nme.5322.
28. White S, Weaver P. Towards imperfection insensitive buckling response of shell structures-shells with plate-like post-buckled responses. *Aeronautical Journal* 2016; **120**(1224):233–253, doi:10.1017/aer.2015.14.
29. White S, Raju G, Weaver P. Initial post-buckling of variable-stiffness curved panels. *Journal of the Mechanics and Physics of Solids* 2014; **71**:132 – 155, doi:http://dx.doi.org/10.1016/j.jmps.2014.07.003.
30. Liang K, Ruess M, Abdalla M. The Koiter-Newton approach using von Karman kinematics for buckling analyses of imperfection sensitive structures. *Computer Methods in Applied Mechanics and Engineering* 2014; **279**:440–468, doi:10.1016/j.cma.2014.07.008.
31. Liang K, Abdalla M, Gürdal Z. A Koiter-Newton approach for nonlinear structural analysis. *International Journal for Numerical Methods in Engineering* 2013; **96**(12):763–786, doi:10.1002/nme.4581.
32. Zagari G, Madeo A, Casciaro R, De Miranda S, Ubertini F. Koiter analysis of folded structures using a corotational approach. *International Journal of Solids and Structures* 2013; **50**(5):755–765, doi:10.1016/j.ijsolstr.2012.11.007.
33. Madeo A, Groh R, Zucco G, Weaver P, Zagari G, Zinno R. Post-buckling analysis of variable-angle tow composite plates using Koiter's approach and the finite element method. *Thin-Walled Structures* 2017; **110**:1–13, doi: 10.1016/j.tws.2016.10.012.
34. Barbero E, Madeo A, Zagari G, Zinno R, Zucco G. Koiter asymptotic analysis of folded laminated composite plates. *Composites Part B: Engineering* 2014; **61**:267–274, doi:10.1016/j.compositesb.2014.01.045. Cited By 6.
35. Rahman T, Jansen E. Finite element based coupled mode initial post-buckling analysis of a composite cylindrical shell. *Thin-Walled Structures* 2010; **48**(1):25–32, doi:10.1016/j.tws.2009.08.003.
36. Rahman T, Ijsselmuiden S, Abdalla M, Jansen E. Postbuckling analysis of variable stiffness composite plates using a finite element-based perturbation method. *International Journal of Structural Stability and Dynamics* 2011; **11**(4):735–753, doi:10.1142/S0219455411004324.

37. Casciaro R, Salerno G, Lanzo A. Finite element asymptotic analysis of slender elastic structures: A simple approach. *International Journal for Numerical Methods in Engineering* 1992; **35**(7):1397–1426, doi: 10.1002/nme.1620350703.
38. Garcea G. Mixed formulation in Koiter analysis of thin-walled beams. *Computer Methods in Applied Mechanics and Engineering* 2001; **190**(26-27):3369–3399.
39. Garcea G, Bilotta A, Madeo A, Casciaro R. *Direct evaluation of the post-buckling behavior of slender structures through a numerical asymptotic formulation*. Springer Verlag, 2014, doi:10.1007/978-94-007-6827-7 10.
40. Lanzo AD, Garcea G. Koiter's analysis of thin-walled structures by a finite element approach. *International Journal for Numerical Methods in Engineering* 1996; **39**(17):3007–3031.
41. Garcea G, Leonetti L, Magisano D, Gonçalves R, Camotim D. Deformation modes for the post-critical analysis of thin-walled compressed members by a Koiter semi-analytic approach. *International Journal of Solids and Structures* 2017; **110-111**:367–384, doi:10.1016/j.ijsolstr.2016.09.010.
42. Garcea G, Madeo A, Casciaro R. The implicit corotational method and its use in the derivation of nonlinear structural models for beams and plates. *J. Mech. Mater. Struct.* 2012; **7**(6):509–539, doi: 10.2140/jomms.2012.7.509.
43. Garcea G, Madeo A, Casciaro R. Nonlinear FEM analysis for beams and plate assemblages based on the implicit corotational method. *J. Mech. Mater. Struct.* 2012; **7**(6):539–574, doi:10.2140/jomms.2012.7.539.
44. Garcea G, Madeo A, Zagari G, Casciaro R. Asymptotic post-buckling FEM analysis using corotational formulation. *International Journal of Solids and Structures* 2009; **46**(2):377–397.
45. Peek R, Kheyrkhahan M. Postbuckling behavior and imperfection sensitivity of elastic structures by the Lyapunov-Schmidt-Koiter approach. *Computer Methods in Applied Mechanics and Engineering* 1993; **108**(3-4):261–279, doi:10.1016/0045-7825(93)90005-I.
46. Garcea G, Trunfio G, Casciaro R. Mixed formulation and locking in path-following nonlinear analysis. *Computer Methods in Applied Mechanics and Engineering* NOV 2 1998; **165**(1-4):247–272.
47. Magisano D, Leonetti L, Garcea G. How to improve efficiency and robustness of the Newton method in geometrically non-linear structural problem discretized via displacement-based finite elements. *Computer Methods in Applied Mechanics and Engineering* 2017; **313**:986 – 1005, doi:http://dx.doi.org/10.1016/j.cma.2016.10.023.
48. Castro SG, Zimmermann R, Arbelo MA, Degenhardt R. Exploring the constancy of the global buckling load after a critical geometric imperfection level in thin-walled cylindrical shells for less conservative knock-down factors. *Thin-Walled Structures* 2013; **72**:76 – 87, doi:http://dx.doi.org/10.1016/j.tws.2013.06.016.

DOI: 10.1002/nme